applied sciences

MDPI

Communication

A Method Based on Blackbody to Estimate Actual Radiation of Measured Cooperative Target Using an Infrared Thermal Imager

Mingyu Yang [1,2], Liang Xu [1,2,*], Xin Tan [1] and Honghai Shen [1,3]

[1] Changchun Institute of Optics, Fine Mechanics and Physics, Chinese Academy of Sciences, Changchun 130033, China; ymy1983@163.com (M.Y.)
[2] Agricultural Hyperspectral Application & Information Database, Changchun 130033, China
[3] Key Laboratory of Airborne Optical Imaging and Measurement, Changchun Institute of Optics, Fine Mechanics and Physics, Chinese Academy of Sciences, Changchun 130033, China
* Correspondence: xuliang_9981@163.com

Abstract: Infrared signature of targets is one important approach for target detection and recognition. When measuring the infrared signature of a target in the atmosphere, it is necessary to take the atmospheric transmittance and atmospheric radiation between the measured target and the observer into account. In this study, a blackbody-based approach for estimating atmospheric transmittance and atmospheric radiation is proposed to improve accuracy. Radiometric calibration is first carried out in the laboratory for the infrared thermal imager to determine the slope and offset used in the linear regression. With a set of different temperatures, radiance of the blackbody and digital number value of images are calculated. Finally, according to the analytical expressions derived, the atmospheric transmittance and atmospheric radiation are determined, and actual radiance for the cooperative target is calculated. Results demonstrate that the uncertainty of the actual radiance of measured cooperative target calculated via the proposed method is lower than that by MODTRAN, from MODTRAN at 5.7% and 16.7%, from proposed method at 2.56% and 10.2% in two experiments.

Keywords: infrared signature; atmospheric transmittance; infrared thermal imager; radiometric calibration

Citation: Yang, M.; Xu, L.; Tan, X.; Shen, H. A Method Based on Blackbody to Estimate Actual Radiation of Measured Cooperative Target Using an Infrared Thermal Imager. *Appl. Sci.* **2023**, *13*, 4832. https://doi.org/10.3390/app13084832

Academic Editor: Vittoria Guglielmi

Received: 5 February 2023
Revised: 17 March 2023
Accepted: 28 March 2023
Published: 12 April 2023

1. Introduction

With the further development of infrared focal plane arrays (IRFPA), infrared remote sensing techniques play an important role in many fields, especially in multiple military cases for aerospace vehicles [1–4]. Infrared signature has been demonstrated much during the last few years in feature acquisition and recognition of targets, which can provide signature information of targets such as radiance and intensity [5–7], for different vehicles usually represent different infrared signature.

At present, the research on the infrared radiation characteristics of targets mainly includes two ways, namely the simulation and the experiment. In the simulation, the mathematical radiation model is first established based on the state and the environment of targets. Then, according to the radiation formation mechanism of targets, each component that influences the radiation characteristic of the target is analyzed and calculated theoretically [8–13]. Although the simulation is widely used in the study of the infrared characteristics, due to the fact that they are not subject to the site and cost, the accuracy and effectiveness cannot be easily verified. In contrast, the experiment that measures and inverses the actual radiation of the target with a radiometrically calibrated infrared measuring system is the direct and the only means to obtain and verify the radiation characteristics of the measured target [14,15]. In experiments, infrared signature measurement of targets usually consists of three steps: (1) radiometric calibration for the infrared thermal imager, which aims at quantifying the relationship between the radiation received and the output digital number (DN); (2) estimation of the emission and reflection from the ground and

the atmospheric effects, such as atmospheric transmittance and path radiation, which can be predicted by software like MODTRAN; (3) inversion of the radiation characteristics using a model of radiation measurement, according to the target material surface emissivity, transmittance and so on. In both approaches mentioned above, the influence caused by the atmosphere must be inevitably corrected, especially for long range targets. However, the estimation of atmospheric parameters and the atmospheric radiation, nowadays, mainly depends on atmospheric transmission radiative transfer software such as LOWTRAN, MODTRAN, and FASCODE, of which the uncertainty is merely approximately 20–30% which is far from enough in engineering application.

In this work, a method of infrared radiation measurement based on blackbody or an object served as a blackbody for cooperative targets is proposed, based on which the atmospheric transmittance and the atmospheric radiation are estimated and the actual radiation of the measured cooperative target is calculated with lower uncertainty. The proposed method can be considered as an alternative for practical scenes when measuring cooperative targets in engineering applications.

2. Materials and Methods

2.1. MODTRAN

Moderate Resolution Atmospheric Transmission radiative transfer code and algorithm (MODTRAN) [16], developed by the U.S. Air Force Research Lab, is widely used to calculate various atmospheric radiative transfer parameters under complex atmospheric conditions from 0 to 50,000 cm^{-1}, such as transmittance, et al. Models of atmosphere in MODTRAN can be defined by users according to the theoretical calculation or measured data, which makes the simulation and use of MODTRAN particularly flexible. In addition, MODTRAN includes representative models of atmosphere, aerosol, cloud, and rain, and various complex geometric conditions such as horizontal, vertical, inclined upward, and downward transmission, which makes MODTRAN a powerful tool in the calculation of atmospheric radiative transfer parameters.

Although MODTRAN software provides default parameters for most settings, it would be best if measured data is input in order to approximate the real situation. For atmospheric parameters collection, cloud and aerosol micro lidar to determine the visibility and aerosol extinction profile, automatic sun tracking photometer to measure total atmospheric transmittance and total water vapor, and meterological station to collect the temperature, humidity, wind, pressure, et al., are often employed in the process of atmospheric parameters measurement. Figure 1 shows the workflow for the correction of atmospheric transmission via MODTRAN using measured atmospheric parameters.

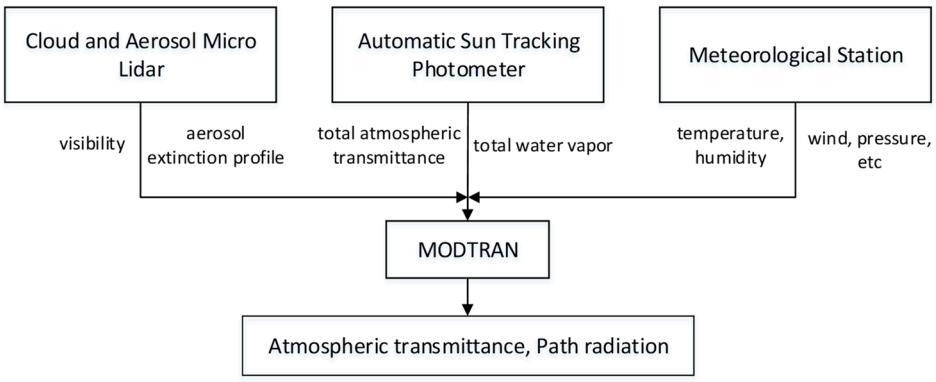

Figure 1. Workflow for MODTRAN software using measured atmospheric parameters.

2.2. Theory of Infrared Radiation

The radiation obtained by an infrared thermal imager mainly includes three parts: the self-radiation of the measured target, reflected environmental radiation, and atmospheric

radiation [17]. The equivalent radiance from the surface of an opaque target by an infrared thermal imager can be expressed as:

$$L_\lambda(T_r) = \tau_{a\lambda}\varepsilon_\lambda L_{b\lambda}(T_0) + \tau_{a\lambda}(1-\alpha_\lambda)L_{b\lambda}(T_u) + \varepsilon_{a\lambda}L_{b\lambda}(T_a) \quad (1)$$

where T_r is the radiation temperature measured with the infrared thermal imager, T_0 is the surface temperature of the object, T_u is the ambient temperature, T_a is the atmospheric temperature, ε_λ is the surface emissivity of the measured object, $\varepsilon_{a\lambda}$ is the atmospheric emissivity, $\tau_{a\lambda}$ is the atmospheric transmittance, α_λ is the surface absorptance of the object, and $L_{b\lambda}$ denotes the radiance emitted by the blackbody at wavelength λ.

The corresponding irradiance of entrance pupil for the infrared thermal imager is:

$$E_\lambda = A_0 d^{-2} L_\lambda = A_0 d^{-2}[\tau_{a\lambda}\varepsilon_\lambda L_{b\lambda}(T_0) + \tau_{a\lambda}(1-\alpha_\lambda)L_{b\lambda}(T_u) + \varepsilon_{a\lambda}L_{b\lambda}(T_a)] \quad (2)$$

where A_0 is the visible area of the target corresponding to the minimum space angle of the thermal imager, d is the distance between the target and the thermal imager, and usually $A_0 d^{-2}$ is considered as a constant.

Radiation power of the infrared thermal imager received for a certain wavelength is:

$$P_\lambda = E_\lambda A_r \quad (3)$$

where A_r is the area of lens of the thermal imager.

Without considering stray radiation, which can be minimized via high projection material and cold aperture, the total radiation of the thermal imager received P_T is:

$$P_T = \tau_{op} P_\lambda \quad (4)$$

where τ_{op} is the transmittance of optical systems.

The response voltage signal V_s is referred according to [18] as:

$$V_s = g(R_\lambda P_T + V_0) \quad (5)$$

where R_λ is the spectral responsivity of the infrared thermal imager, which is a constant for a certain infrared thermal imager; V_0 is the DC bias voltage; and g is the response gain used to amplify the signal.

$$\begin{aligned} V_s = \; & A_r A_0 d^{-2}\tau_{op} g\{\tau_{a\lambda}[\varepsilon_\lambda \textstyle\int_{\lambda_1}^{\lambda_2} R_\lambda L_{b\lambda}(T_0)d\lambda + (1-\alpha_\lambda)\int_{\lambda_1}^{\lambda_2} R_\lambda L_{b\lambda}(T_u)d\lambda] \\ & + \varepsilon_{a\lambda}\textstyle\int_{\lambda_1}^{\lambda_2} R_\lambda L_{b\lambda}(T_a)d\lambda\} + gV_0 \end{aligned} \quad (6)$$

Let

$$K = A_r A_0 d^{-2}\tau_{op} g \quad (7)$$

$$f(T) = \int_{\lambda_1}^{\lambda_2} R_\lambda L_{b\lambda}(T)d\lambda \quad (8)$$

Equation (6) is then simplified for:

$$V_s = K\{\tau_{a\lambda}[\varepsilon_\lambda f(T_0) + (1-\alpha_\lambda)f(T_u)] + \varepsilon_{a\lambda}f(T_a)\} + gV_0 \quad (9)$$

When the surface of the measured target can be treated as a gray body, according to Kirchhoff's law ($\varepsilon_\lambda = \alpha_\lambda$ and $\varepsilon_{a\lambda} = 1 - \tau_{a\lambda}$) and especially when the measured target is a blackbody, Equation (9) is simplified for:

$$V_s = K\{\tau_{a\lambda}f(T_0) + \varepsilon_{a\lambda}f(T_a)\} + gV_0 \quad (10)$$

As the output of the infrared thermal imager, also called the digital number (DN), is usually proportion to V_s [19], Equation (10) is transformed into:

$$G_s = k\{\tau_{a\lambda}[\varepsilon_\lambda f(T_0) + (1-\alpha_\lambda)f(T_u)] + \varepsilon_{a\lambda} f(T_a)\} + G_0 \quad (11)$$

When the measured target and the infrared thermal imager are determined, the coefficients become fixed values; the actual radiance of the measured target is:

$$f(T_0) = \frac{\frac{G_s - G_0}{k} - \varepsilon_{a\lambda} f(T_a)}{\tau_{a\lambda}} - (1-\alpha_\lambda) f(T_u) \quad (12)$$

2.3. Model of Radiometric Calibration and Infrared Thermal Imager

One of the most commonly used approaches of radiometric calibration for infrared thermal imager is that setting a blackbody source of large area to completely cover the field-of-view (FOV) of the infrared thermal imager [20–22], as shown in Figure 2.

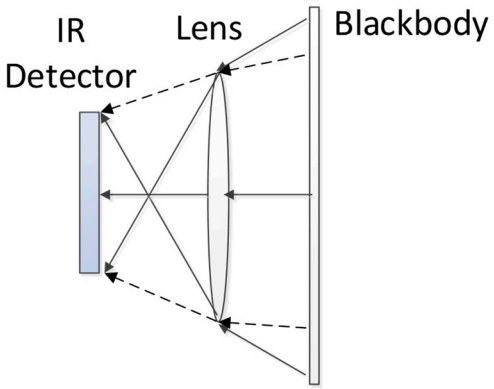

Figure 2. Schematic diagram of the radiometric calibration.

Since the calibration is usually carried out in the laboratory and the thermal imager is very close to the blackbody, the influence of the atmosphere can be ignored, $\varepsilon_\lambda = \alpha_\lambda = 1$, $\tau_{a\lambda} = 1$ and $\varepsilon_{a\lambda} = 0$. As a result, Equation (11) is simplified as:

$$G_s = k f(T_0) + G_0 \quad (13)$$

where $f(T_0)$ can be calculated according to Planck's law of radiation:

$$f(T_0) = \frac{1}{\pi}\int_{\lambda_1}^{\lambda_2} \frac{C_1 \lambda^{-5}}{e^{C_2/\lambda T_0} - 1} d\lambda \quad (14)$$

In Equation (14), C_1 and C_2 are called the first and second radiation constants, respectively, with values $C_1 = 2\pi hc^2 = 3.742 \times 10^{-16}\ \mathrm{W \cdot m^2}$ and $C_2 = hc/k_B = 1.4388 \times 10^{-2}\ \mathrm{m \cdot K}$, where fundamental constants c (2.997×10^8 m/s), h (6.626×10^{-34} J s), and k_B (1.381×10^{-23} J/K) are the speed of light in vacuo, Planck's constant, and Boltzmann's constant, respectively.

In the process of radiometric calibration, it is necessary to keep laboratory conditions and thermal imager parameters unchanged. Nonuniformity correction (NUC) is often applied to make the response of each pixel identical. The procedure of radiometric calibration for an infrared thermal imager is as follows.

1. Turn off the auto gain function of the infrared thermal imager, and set focus to infinity;
2. Apply NUC to the blackbody source;
3. Save frames of image when the temperature of blackbody source is completely stable, then average the saved images to reduce random noises;
4. Collect DN value for the averaged images of different temperatures;

5. Calculate the radiance according to Equation (14);
6. Change the temperature of the blackbody and repeat the steps 3–5 until all temperatures are measured;
7. Fit DN value and the radiance in Equation (13) by the least square method.

The infrared thermal imager and the blackbody source used for radiometric calibration are shown in Figure 3.

(**a**) (**b**)

Figure 3. The infrared thermal imager and the blackbody source. (**a**) Infrared thermal imager; (**b**) Blackbody source.

The properties of the infrared thermal imager and the blackbody source are listed in Tables 1 and 2, respectively.

Table 1. Properties of the infrared thermal imager.

Parameter	Value
Manufacturer	FLIR Systems
Model	MINICORE-600Z
Band Range	3.7–4.8 μm
Resolution	640 × 512 pixel
Pixel Size	15 μm × 15 μm
Output Bit	14 bit
F#	F4
Focus	30–600 mm continuous zooming
Cooling Type	Stirling cooling

Table 2. Properties of the blackbody source.

Parameter	Value
Manufacturer	CI Systems
Model	SR800-12LT
Size	305 mm × 305 mm
Temperature range	−40–150 °C
Emissivity	0.97 ± 0.02
Uniformity	±0.03 °C

2.4. The Proposed Blackbody-Based Method

Although MODTRAN software is widely used to estimate the transmittance, atmospheric radiation, and so on, it is only suitable for theoretical analysis not practical scenes, for MODTRAN is mainly based on the U.S atmospheric parameters which cannot represent the actual condition in the other places, especially in cities with heavy pollution. The proposed method can be considered as an alternative for practical scenes. The atmospheric

transmittance and atmospheric radiation can both be derived from Equation (11) by setting two different temperatures denoted as T_{0H} and T_{0L} as follows:

$$G_{sH} = k\{\tau_{a\lambda}[\varepsilon_\lambda f(T_{0H}) + (1-\alpha_\lambda)f(T_u)] + \varepsilon_{a\lambda} f(T_a)\} + G_0 \quad (15)$$

$$G_{sL} = k\{\tau_{a\lambda}[\varepsilon_\lambda f(T_{0L}) + (1-\alpha_\lambda)f(T_u)] + \varepsilon_{a\lambda} f(T_a)\} + G_0 \quad (16)$$

Hence, the atmospheric transmittance and atmospheric radiation can be derived by Equation (15) minus Equation (16) and Equation (15) plus Equation (16) as follows:

$$\tau_{a\lambda} = \frac{G_{sH} - G_{sL}}{k[\varepsilon_\lambda f(T_{0H}) - \varepsilon_\lambda f(T_{0L})]} \quad (17)$$

$$\varepsilon_{a\lambda} f(T_a) = \frac{1}{2} \cdot \{\frac{G_{sH} + G_{sL} - 2G_0}{k} - \tau_{a\lambda}[\varepsilon_\lambda f(T_{0H}) + \varepsilon_\lambda f(T_{0L}) + 2(1-\alpha_\lambda)f(T_u)]\} \quad (18)$$

Figure 4 shows the workflow for correction of atmospheric transmission using the proposed approach.

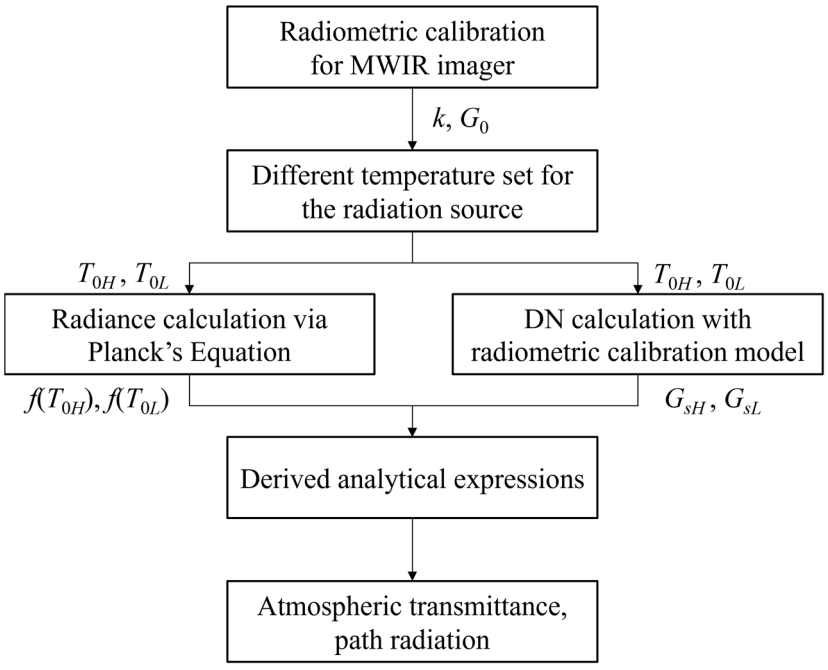

Figure 4. Workflow for the proposed method.

3. Results

3.1. Radiometric Calibration for the Infrared Thermal Imager

In the process of radiometric calibration for the infrared thermal imager, two-point NUC is applied to ensure the uniformity of images from the blackbody source. In addition, we use a DALSA X64-CL iPro image acquisition card to grab 100 image frames for each temperature, and set temperatures of the blackbody increasing from 35 to 115 degrees C at interval of 5 degrees C, with DN value of pixel (320,256) collected. The radiance calculated according to Planck' law of radiation and corresponding DN value are shown in Table 3.

Table 3. Radiance and DN value collected in the radiometric calibration.

Temperature/°C	Radiance/W·m^{-2}·str^{-1}	DN Value
35	2.4764	1986
40	2.9356	2257
45	3.4627	2584
50	4.0649	2979
55	4.7501	3399
60	5.5267	3900
65	6.4034	4491
70	7.3896	5162
75	8.4950	5904
80	9.7299	6722
85	11.1051	7668
90	12.6318	8717
95	14.3216	9880
100	16.1866	11,295
105	18.2395	12,658
110	20.4933	15,106
115	22.9614	15,114

Table 3 indicates that the DN value is of little increase during the temperature increasing from 110 degrees C to 115 degrees C. Considering the 14-bit output of the thermal imager, it can be concluded that the DN value has reached a saturation point around 110 degrees C. Therefore, data from 110 to 115 degrees C is removed for the least square, and only data from 35 to 105 degrees C is used. The result of the radiometric calibration under the condition of 2 ms integration time, 300 mm focal length, is given:

$$G_s = 679f(T_0) + 194 \tag{19}$$

with the fitted straight line using least square method shown in Figure 5.

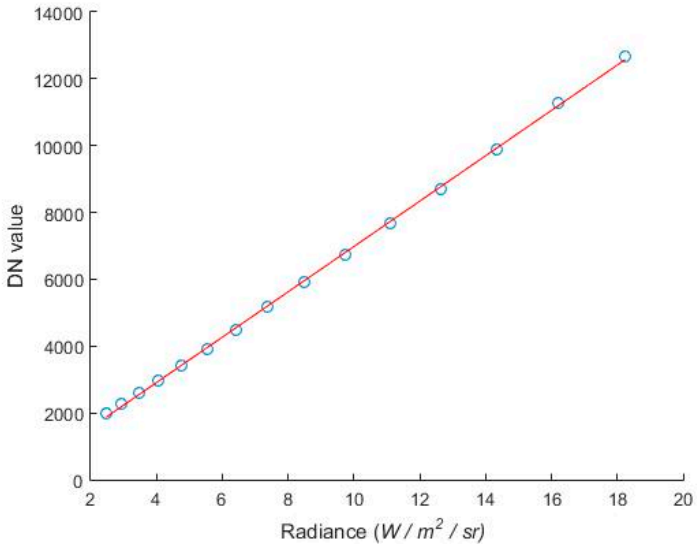

Figure 5. Fitted straight line with the least square method.

3.2. Experiments

We conduct an infrared radiation measuring experiment for the blackbody source in different temperatures. The blackbody source is settled horizontally 30 m away from the infrared thermal imager, with temperature increasing from 65 to 105 degrees C at intervals of 10 degrees C, as shown in Figure 6.

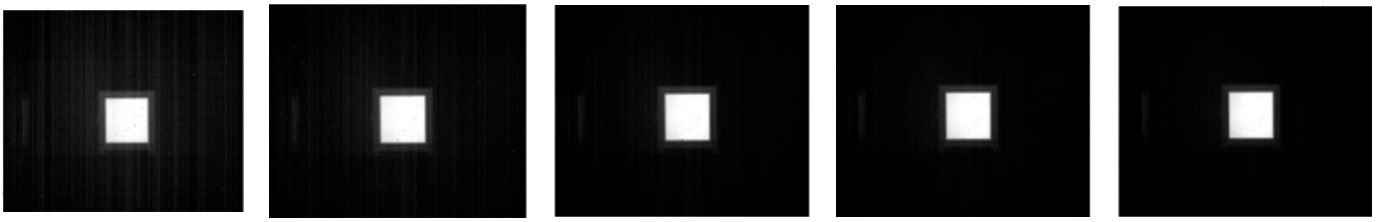

(**a**) (**b**) (**c**) (**d**) (**e**)

Figure 6. Blackbody source in field test with different temperatures in degree C: (**a**) 65; (**b**) 75; (**c**) 85; (**d**) 95; (**e**) 105.

The radiance calculated according to Planck' law of radiation and corresponding DN value are listed in Table 4.

Table 4. Radiance and DN value for the blackbody test.

Temperature/°C	Radiance/W·m^{-2}·str^{-1}	DN Value
65	6.4034	4072
75	8.4950	5298
85	11.1051	6764
95	14.3216	8605
105	18.2395	11,207

According to Equations (17) and (18) the atmospheric transmittance $\tau_{a\lambda}$ and atmospheric radiation $\varepsilon_{a\lambda}f(T_a)$ can be calculated through least square fitting in order to reduce error, values of which are approximately 88.8% and 0.0239 W/m^2/sr. In comparison with MODTRAN, the atmospheric parameters used for the blackbody test are listed in Table 5.

Table 5. Atmospheric parameters used in MODTRAN for the blackbody test.

Atmospheric Parameters	Value
Atmospheric profile	Mid-latitude summer
Altitude of observer (km)	0.216
Visibility (km)	13
Humidity (%)	54
Temperature (°C)	20
Atmospheric path	horizontal
Distance from observer to target (m)	30
CO_2 mixing ratio (ppmv)	370

Input these parameters listed in Table 5 into MODTRAN, the atmospheric transmittance and atmospheric radiation are 83.9% and 0.0352 W/m^2/sr, respectively. With all the parameters given above, the infrared radiation of targets can be calculated by Equation (12). The comparison of inversion results with the derivation from the analytical expression and with MODTRAN are given in Table 6. It is obvious that the inversion results derived by the expression in each row are closer to the actual radiance of the blackbody than that by MODTRAN, with the maximal error of 2.56% and 5.7% by the derivation from the analytical expression and by MODTRAN, respectively.

To extend the verification to other tests, we also carried out a field test for a fan-shaped infrared target. Due to the relatively small size of the blackbody, we cannot acquire enough pixels over a long distance in some cases. The target with a bigger fan-shaped infrared target is used in the experiment, which consists of 10 pieces of heating plates, each with an 18-degree central angle, the radius of 2.25 m, and the surface emissivity of 0.52. The fan-shaped target is shown in Figure 7, with the aluminum box of the temperature controller.

Table 6. Comparison of inversion results for the blackbody source.

Temp (°C)	DN Value	Actual Radiance ($W/m^2/sr$)	Radiance with MODTRAN ($W/m^{2/}sr$)	Error with MODTRAN (%)	Radiance with Derivation ($W/m^2/sr$)	Error with Derivation (%)
65	4072	6.4034	6.7654	5.6	6.4348	0.48
75	5298	8.4950	8.9174	4.9	8.4696	0.29
85	6764	11.1051	11.4908	3.4	10.9010	1.83
95	8605	14.3216	14.7224	2.7	13.9552	2.55
105	11,207	18.2395	19.2899	5.7	18.2731	0.18

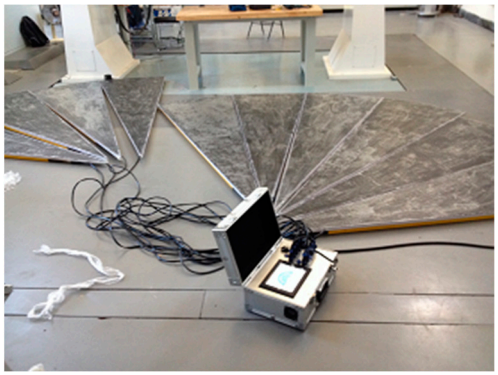

Figure 7. Heating plates used in the field test.

Two pieces of plates are chosen in the experiment, with the temperature increasing from 35 to 50 degrees C at intervals of 3 degrees C and with the ambient temperature of 28 degrees C, shown in Figure 8.

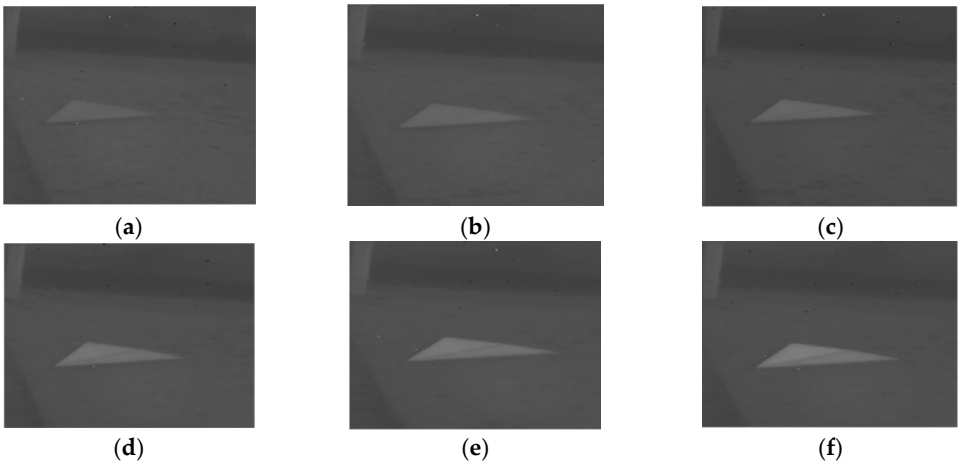

Figure 8. Heating plates with different temperatures in degree C: (**a**) 35; (**b**) 38; (**c**) 41; (**d**) 44; (**e**) 47; (**f**) 50.

The atmospheric parameters for the fan-shaped target test are listed in Table 7.

The transmittance and atmospheric radiation are calculated by Equation (12) with values of 73.3% and 1.17 $W/m^2/sr$, while by MODTRAN with values of 72.3% and 1.34 $W/m^2/sr$, respectively. Table 8 shows the comparison of inversion results for the two hearting plates, indicating that for each row, the radiance derived from the analytical expression is also closer to the actual radiance than that from MODTRAN over a relatively long distance, with the maximal error of 10.2% and 16.7% by the derivation from the analytical expression and by MODTRAN, respectively.

Table 7. Atmospheric parameters used in MODTRAN for the fan-shaped target test.

Atmospheric Parameters	Value
Atmospheric profile	Mid-latitude summer
Altitude of observer (km)	0.22
Visibility (km)	13
Humidity (%)	45
Temperature (°C)	28
atmospheric path	slant
distance from observer to target (m)	1560
CO_2 mixing ratio (ppmv)	370

Table 8. Comparison of inversion results for heating plates.

Temp (°C)	DN Value	Actual Radiance ($W/m^2/sr$)	Radiance with MODTRAN ($W/m^2/sr$)	Error with MODTRAN (%)	Radiance with Derivation ($W/m^2/sr$)	Error with Derivation (%)
35	1630	2.4764	2.0611	−16.7	2.4789	0.10
38	1701	2.7442	2.3392	−14.8	2.7532	0.33
41	1823	3.0354	2.8171	−7.2	3.2246	6.2
44	1944	3.3515	3.2911	−1.8	3.6922	10.2
47	1978	3.6941	3.4243	−7.3	3.8235	3.5
50	2041	4.0649	3.6711	−9.7	4.0669	0.05

4. Discussion

For long distance infrared signature of targets in the field, the inversion uncertainty is mainly affected by (1) the uncertainty of the radiometric calibration, (2) the uncertainty of the estimation for the atmospheric transmittance and atmospheric radiation, and (3) the uncertainty of the environmental condition changes in the field, such as temperature, wind, etc., other than that in the laboratory. Among these factors mentioned above, the uncertainty in the radiometric calibration, i.e., values of k and G_0 in Equation (13), under current measuring conditions is approximately 6% for a medium-wave infrared thermal imager [22]. The uncertainty in the estimation of the atmospheric transmittance and atmospheric radiation, depending on meteorological equipment and MODTRAN, is about 20–30%; and the environmental differences between the field and the laboratory is usually 10%. As a result, the uncertainty of the measurement for the infrared thermal imager can be calculated by the root mean square of the three factors listed above, approximately 23.2–32.2%. In our experiments, the inversion uncertainty derived from the analytical expression and by MODTRAN is 2.56%, 10.2% and 5.7%, 16.7%, respectively, both of which are acceptable according to the above analysis. It is obvious that the uncertainty derived from the analytical expressions is lower than that by MODTRAN for cooperative targets, i.e., targets that can be easily placed a blackbody or an object that served as a blackbody nearby. However, for non-cooperative targets such as an enemy vehicle, we can only employ MODTRAN to estimate the radiation of targets theoretically.

5. Conclusions

In this paper, a blackbody-based approach for estimating the actual radiation of measured cooperative target is proposed. Firstly, radiometric calibration is carried out in the laboratory for the infrared thermal imager to determine the slope and offset used in the linear regression. Then, the radiance of the blackbody and digital number value of images are calculated with a set of different temperatures. Finally, according to the analytical expressions derived the atmospheric transmittance and atmospheric radiation are determined, and actual radiance for the cooperative target is calculated. Lab and field tests demonstrate that the uncertainty of the actual radiance of measured cooperative target calculated via the proposed method is lower than that by MODTRAN, which can be considered as an alternative for practical scenes when measuring cooperative targets in engineering application. Future studies will mainly focus on lowering the uncertainty

for non-cooperative targets over long distances, which aims to reduce the impact of the atmospheric transmission to improve furtherly the infrared radiation of measured targets.

Author Contributions: Conceptualization, M.Y.; methodology, M.Y.; software, M.Y.; validation, M.Y., L.X. and X.T.; formal analysis, M.Y.; investigation, H.S.; resources, H.S.; data curation, M.Y.; writing—original draft preparation, M.Y.; writing—review and editing, L.X. and X.T.; visualization, M.Y.; supervision, X.T.; project administration, L.X.; funding acquisition, L.X. All authors have read and agreed to the published version of the manuscript.

Funding: Science and Technology Resources Shared Services Platform Construction of JiLin Province (No.20230505009ZP).

Institutional Review Board Statement: Not applicable.

Informed Consent Statement: Not applicable.

Data Availability Statement: The data presented in this study are available from Tables 3–8.

Conflicts of Interest: The authors declare no conflict of interest.

References

1. Jacobs, A. *Thermal Infrared Characterization of Ground Targets and Backgrounds*; SPIE Optical Engineering Press: Washington, DC, USA, 1996; pp. 140–149.
2. Mahulikar, P.; Sonawane, R.; Arvind Rao, G. Infrared signature studies of aerospace vehicles. *Prog. Aerosp. Sci.* **2007**, *43*, 218–245. [CrossRef]
3. Zhao, B.; Xiao, S.; Lu, H.; Wu, D. Modeling and simulation of infrared signature of remote aerial targets. In Proceedings of the 2017 10th International Congress on Image and Signal Processing, BioMedical Engineering and Informatics (CISP-BMEI), Shanghai, China, 14–16 October 2017; pp. 1–5. [CrossRef]
4. Zhang, Y.-C.; Chen, Y.-M.; Fu, X.-B.; Luo, C. The research on the effect of atmospheric transmittance for the measuring accuracy of infrared thermal imager. *Infrared Phys. Technol.* **2016**, *77*, 375–381. [CrossRef]
5. Leslie, P.; Furxhi, O.; Short, R.; Grimming, R.; Driggers, R. Mid-Wave and Long-Wave Infrared Signature Model and Measurements of Power Lines Against Atmospheric Path Radiance. In Proceedings of the 2021 IEEE Research and Applications of Photonics in Defense Conference (RAPID), Miramar Beach, FL, USA, 2–4 August 2021; pp. 1–2. [CrossRef]
6. Talghader, J.J.; Gawarikar, A.S.; Shea, R.P. Spectral selectivity in infrared thermal detection. *Light. Sci. Appl.* **2012**, *1*, 6–16. [CrossRef]
7. Qiu, H.; Hu, L.; Zhang, Y.; Lu, D.; Qi, J. Absolute Radiometric Calibration of Earth Radiation Measurement on FY-3B and Its Comparison With CERES/Aqua Data. *IEEE Trans. Geosci. Remote Sens.* **2012**, *50*, 4965–4974. [CrossRef]
8. Poline, M.; Rebrov, O.; Larsson, M.; Zhaunerchyk, V. Theoretical studies of infrared signatures of proton-bound amino acid dimers with homochiral and heterochiral moieties. *Chirality* **2020**, *32*, 359–369. [CrossRef] [PubMed]
9. Liu, J.; Yue, H.; Lin, J.; Zhang, Y. A Simulation Method of Aircraft Infrared Signature Measurement with Subscale Models. *Procedia Comput. Sci.* **2019**, *147*, 2–16. [CrossRef]
10. Knežević, D.M.; Matavulj, P.S.; Nikolić, Z.M. Modeling of aircraft infrared signature based on comparative tracking. *Optik* **2021**, *225*, 165782. [CrossRef]
11. Zhang, D.; Bai, L.; Wang, Y.; Lv, Q.; Zhang, T. An improved SHDOM coupled with CFD for simulating infrared radiation signatures of rocket plumes. *Infrared Phys. Technol.* **2022**, *122*, 104054. [CrossRef]
12. Xu, M.; Bu, X.; Yu, J.; He, Z. Spinning projectile's attitude measurement with LW infrared radiation under sea-sky background. *Infrared Phys. Technol.* **2018**, *90*, 214–220. [CrossRef]
13. Haq, F.; Huang, J. Parametric design and IR signature study of exhaust plume from elliptical-shaped exhaust nozzles of a low flying UAV using CFD approach. *Results Eng.* **2022**, *13*, 100320. [CrossRef]
14. Cheng, W.; Wang, Z.; Zhou, L.; Shi, J.; Sun, X. Infrared signature of serpentine nozzle with engine swirl. *Aerosp. Sci. Technol.* **2019**, *86*, 794–804. [CrossRef]
15. Ata, Y.; Nakiboğlu, K.C. IR signature estimation of an object or a target by taking into account atmospheric effects. *Opt. Commun.* **2010**, *283*, 3901–3910. [CrossRef]
16. Berk, A.; Anderson, G.P.; Bernstein, L.S.; Acharya, P.K.; Dothe, H.; Matthew, M.W.; Adler-Golden, S.M.; Chetwynd, J.H., Jr.; Richtsmeier, S.C.; Pukall, B.; et al. MODTRAN4 radiative transfer modeling for atmospheric correction. In Proceedings of the SPIE's International Symposium on Optical Science, Engineering, and Instrumentation, Denver, CO, USA, 18–23 July 1999; pp. 348–353. [CrossRef]
17. Ni, N.; Zhang, K.; Hu, J.; Li, L.; Mi, S.; Zhang, Y.; Zhang, Y. Combined Use of Blackbody and Infrared Radiation for Accurate Measurement of Temperature Field of Aluminum Alloys. *Optik* **2022**, *268*, 169763. [CrossRef]
18. Shen, J.; Zhang, Y.; Xing, T. The study on the measurement accuracy of non-steady state temperature field under different emissivity using infrared thermal image. *Infrared Phys. Technol.* **2018**, *94*, 207–213. [CrossRef]

19. Zhang, Y.-C.; Chen, Y.-M.; Luo, C. A method for improving temperature measurement precision on the uncooled infrared thermal imager. *Measurement* **2015**, *74*, 64–69. [CrossRef]
20. Yang, G.; Yu, Y.; Sun, Z.; Li, Z.; Pang, X.; Zhang, T. Radiometric calibration algorithm for high dynamic range infrared imaging system. *Infrared Phys. Technol.* **2023**, *130*, 104607. [CrossRef]
21. Lin, D.; Cui, X.; Wang, Y.; Yang, B.; Tian, P. Pixel-wise radiometric calibration approach for infrared focal plane arrays using mul-tivariate polynomial correction. *Infrared Phys. Technol.* **2022**, *123*, 104110. [CrossRef]
22. Li, Z.; Yu, Y.; Tian, Q.-J.; Chang, S.-T.; He, F.-Y.; Yin, Y.-H.; Qiao, Y.-F. High-efficiency non-uniformity correction for wide dynamic linear infrared radiometry system. *Infrared Phys. Technol.* **2017**, *85*, 395–402. [CrossRef]